Journal of Fluorine Chemistry 131 (2010) 91–97

Contents lists available at ScienceDirect

Journal of Fluorine Chemistry

journal homepage: www.elsevier.com/locate/fluor

Spectroscopic characterization of crystalline AlF_3 phases

R. König [a], G. Scholz [a], K. Scheurell [a], D. Heidemann [a], I. Buchem [a], W.E.S. Unger [b], E. Kemnitz [a,*]

[a] Humboldt-Universität zu Berlin, Institut für Chemie, Brook Taylor-Straße 2, D-12489 Berlin, Germany
[b] BAM Bundesanstalt für Materialforschung und – prüfung, 12200 Berlin, Germany

ARTICLE INFO

Article history:
Received 9 September 2009
Received in revised form 28 October 2009
Accepted 30 October 2009
Available online 11 November 2009

Keywords:
Crystalline aluminium fluorides
Solid state NMR
FT IR
XPS

ABSTRACT

A comprehensive spectroscopic characterization of all known crystalline AlF_3 phases (α-, β-, η-, κ-, θ-AlF_3) is presented for the first time in this study. Beside their X-ray diffraction powder patterns, which were already published in the literature, ^{27}Al and ^{19}F MAS NMR, FT IR and XPS spectroscopic techniques were applied for all phases in a consistent manner. For all phases prepared the utilization of ^{27}Al satellite transition (SATRAS) NMR allowed to determine the quadrupolar parameters of the aluminium sites including their distributions.

In addition, η-AlF_3 was isolated with high phase purity and characterized following a new preparation path different from those known so far in the literature.

1. Introduction

The thermodynamically stable rhombohedral phase of aluminium fluoride, α-AlF_3 [1,2] is well known. Its crystal structure (α-AlF_3, space group $R\bar{3}c$) consists of corner-shared {AlF_6}—octahedra forming a three-dimensional network. As shown by X-ray-diffraction, DSC-Raman and EPR measurements, the matrix undergoes a reversible phase transition of first order at $T_c = 456\,^{\circ}C$ [2–6]. All other phases of aluminium fluoride are metastable and transform into α-AlF_3 at higher temperatures. A complete overview about relations between different AlF_3 phases and their precursor compounds is given in Scheme 1. A variety of starting materials was described in the literature ranging from pure inorganic to organic compounds containing either NH_4^+ cations or pyridine (see Scheme 1).

Beside α-AlF_3 the catalytically active phase β-AlF_3 was extensively studied in the literature [7–10]. For both phases a vibrational analysis was published employing FT IR spectroscopy [11–13] and Raman measurements on α-AlF_3 single crystals [11]. Additional Raman measurements were reported for β-AlF_3 microcrystallites by Boulard et al. [14].

An experimental and theoretical description of the characteristics of the F-K edge absorption X-ray structures (XANES) of α-, β- and an AlF_3-phase, depicted as tetragonal AlF_3 (θ), is given in [15,16]. XPS data of these three AlF_3 phases were reported by Boese et al. [18,19] where charge referencing had been either done to the binding energy of C 1s or Au $4f_{7/2}$ photopeaks. Especially the use of the Au $f_{7/2}$ binding energy has been proven to be useful because C 1s binding energy reference is less reliable with catalytically active materials. Nonetheless we used in this work the more common C 1s binding energy reference (284.8 eV) to be compatible to NIST X-ray Photoelectron Spectroscopy Database [17].

^{19}F and ^{27}Al NMR parameters (chemical shifts and quadrupolar frequency) were exactly determined for α-AlF_3 [20–22]. NMR parameters for β-AlF_3 were only given by Chupas et al. [20] with one ^{27}Al parameter set (ν_Q, η_Q) for the two crystallographically determined aluminium sites.

Herron et al. [23–25] reported the preparation and structures of η-, κ- and θ-AlF_3, estimated their BET surface areas and characterized the catalytic activities for halogen exchange reactions of all aluminium fluoride phases known so far.

Except for α- and β-AlF_3, for all other crystalline aluminium fluoride phases spectroscopic data are missing. This circumstance might be due to the more demanding preparation pathways accompanied by reaction products which are often not phase pure or of less good crystallinity.

In the present study all phases were prepared according to the general pathways depicted in Scheme 1. The following precursor compounds were used: β-$AlF_3{\cdot}3H_2O$ [26] for α-AlF_3, α-$AlF_3{\cdot}3H_2O$ [26] for β-AlF_3, $PyHAlF_4$ (via β-NH_4AlF_4) for κ-AlF_3, $N(C_2H_5)_4AlF_4$ and $N(CH_3)_4AlF_4$, respectively, for θ-AlF_3 and ACF [12,13] for η-AlF_3.

In addition, η-AlF_3 was prepared from $[AlF_2Py_4]^+Cl^-$ [27]. Details of the preparation are described in Section 4.

Having all aluminium fluoride phases available as powders, a comparative spectroscopic investigation of all phases was the main intention of this study. For this purpose FT IR, XPS and particularly ^{27}Al and ^{19}F MAS NMR spectroscopic techniques were applied.

* Corresponding author. Fax: +49 030 2093 7277.
E-mail address: erhard.kemnitz@chemie.hu-berlin.de (E. Kemnitz).

0022-1139/$ – see front matter © 2009 Elsevier B.V. All rights reserved.
doi:10.1016/j.jfluchem.2009.10.015

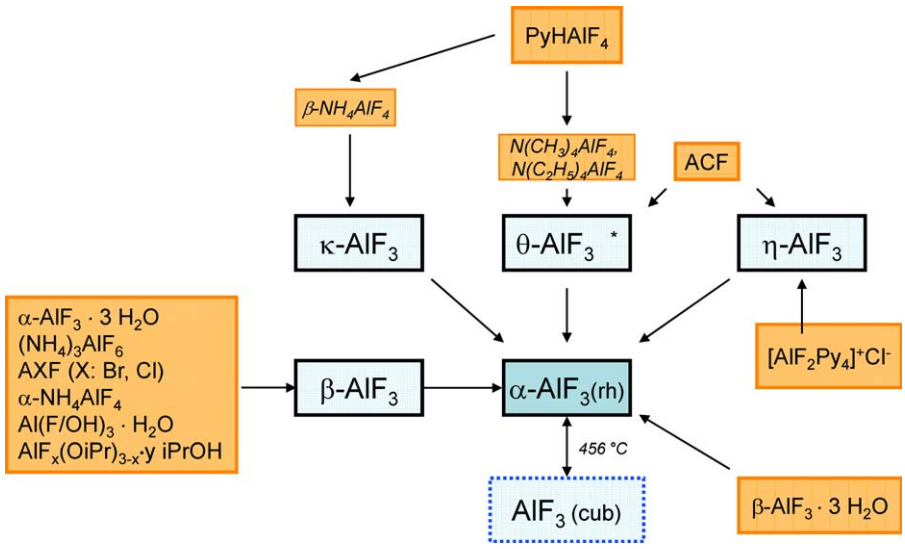

Scheme 1. Relations between different phases of aluminium fluoride and their precursor compounds. *θ-AlF_3 can be prepared along with β-AlF_3 according to [28] also by thermal decomposition of amorphous $AlF_3{}^*xH_2O$; AXF (X: Br, Cl): AlX_yF_{3-y}, $y \approx 0.05–0.25$.

Since corner sharing of AlF_6 octahedra is a common feature of all aluminium fluoride phases and the Al-sites are accordingly very similar, the allocation of differences between their geometric and electronic structures is still a big challenge.

2. Results

Fig. 1 shows the X-ray powder diffractograms of all crystalline AlF_3 phases. Their powder patterns are in agreement with those published in the literature [25] and can be clearly distinguished. All space groups are known and listed together with the number of crystallographically different Al- and F-sites, characteristic bond distances and PDF-entries, if available, in Table 1.

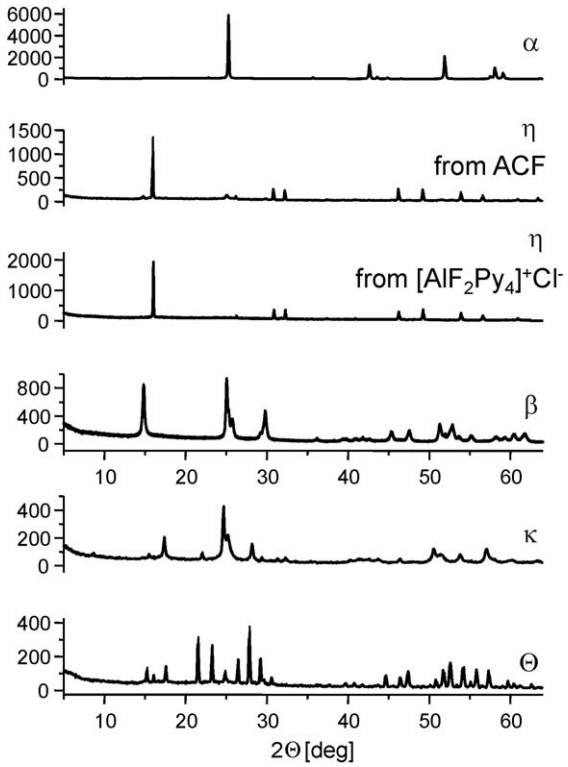

Fig. 1. X-ray powder diffractograms of all crystalline AlF_3 phases known so far. The labelling of the phases is given directly in the figure.

The rhombohedral phase, α-AlF_3, transforms reversibly to the cubic ReO_3 polymorph [2–6]. β-AlF_3, well known for use in catalysis [7–10], is related to the hexagonal tungsten bronze (HTB) structure. Beside α-AlF_3, only the so called η-AlF_3 phase with cubic pyrochlore structure [24] has one crystallographic Al – and one F – site (see Table 1). The key structural feature of the η-phase is the presence of clusters of four corner-shared tetrahedrally disposed AlF_6 octahedra. The structure of κ-AlF_3 possesses many similarities to tetragonal tungsten bronzes K_xWO_3 [24]. Linear channels through the crystal are found comprised of three-, four- and five rings of corner-shared AlF_6 octahedra. The most complex structure is formed by θ-AlF_3 [24,28]. Four different Al-sites and actually seven different F-sites are arranged in rings of five, four or three AlF_6 octahedra forming an undulating 3D channel system (see also Table 1). Drawings of the structures of η-, θ- and κ-AlF_3 together with XRD powder patterns are given by Herron and Farneth [25]. Compared to those diffractograms the signal to noise ratio presented here (Fig. 1) is distinctly better for all samples, but especially for θ-AlF_3.

For η-AlF_3 a new preparation path was found following the thermal decomposition of AlF_2Py_4Cl (see Scheme 1 and Section 4). In contrast to the preparation via ACF (see Scheme 1) a very phase

Table 1
Structures of crystalline AlF_3 phases.

Phase	Space group[a]	Nr. of cryst. different		R(Al-F) [pm][b]	PDF entry[c]
		Al-sites	F-sites		
α-AlF_3	$R\bar{3}c$	1	1	179.7	80-1007
η-AlF_3	$Fd\bar{3}m$	1	1	180.3	Not available
β-AlF_3	Cmcm	2	4	179.6 180.2	84-1672
κ-AlF_3	P4/mbm	2	5	175.1 182.8	83-0719
θ-AlF_3	P4/nmm	4	7	175.1 186.8	83-0717

[a] Le Bail and Calvayrac [34] and references therein.
[b] If different bond distances exist, the smallest and largest Al–F bonds are given.
[c] Ref. [35].

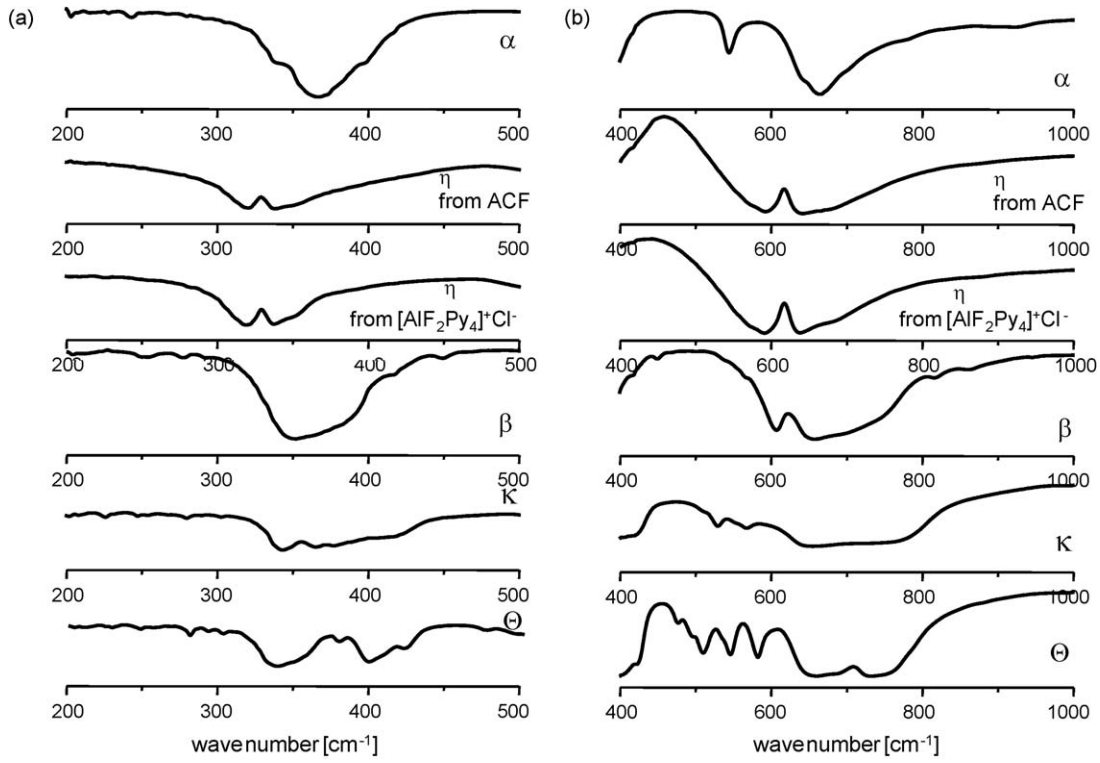

Fig. 2. Transmission IR spectra of all AlF_3 phases: (a) far IR range (200–500 cm^{-1}) and (b) middle IR range (400–1000 cm^{-1}).

pure sample was isolated applying the new synthesis route. However, the cooling regime after heating under Schlenk conditions has a crucial influence on the XRD powder pattern. Cooling down slowly in the furnace results in very pure η-AlF_3 (see Fig. 1). A sudden quenching results in a more heterogeneous phase with additional reflections in XRD caused by texture effects (see Fig. S1).

The transmission IR spectra of all phases are depicted in Fig. 2a (far IR) and b (middle IR). A detailed vibrational analysis of α- and β-AlF_3 [11] showed the presence of mainly bending F–Al–F (and Al–F–Al) vibrations in the far IR range up to 400 cm^{-1}, and predominantly stretching F–Al vibrations above 500 cm^{-1}. Due to the structural affinity of all AlF_3 phases, that is a corner sharing of AlF_6 octahedra, these previously published findings for α- and β-AlF_3 can be essentially transferred to the IR spectra of all phases (see Fig. 2).

The vibrational bands of the two η-AlF_3-samples are comparable, however, the bands of η-AlF_3 prepared from AlF_2Py_4Cl are slightly more narrow as expected.

According to the increased structural diversity in κ- and θ-AlF_3 (see also Table 1) the number of bending as well as stretching frequencies is enlarged and more clearly distinguishable. FT Raman measurements on AlF_3 powders were not successful due to strong fluorescence effects.

More local structural peculiarities can be discovered applying ^{27}Al and ^{19}F MAS NMR spectroscopy. Although a rotation frequency of 25 kHz was applied the presence of possibly different fluorine sites, as shown by XRD, cannot be resolved by ^{19}F MAS NMR (cf. Fig. 3). The positions of all ^{19}F signals are found at $\delta_{19F} \sim -173$ ppm but strong homonuclear dipolar couplings prevent their further resolution (see Table 2). Except for θ-AlF_3, the fluorine spectra of all other phases are very similar and therefore only the spectrum of α-AlF_3 is given exemplarily in Fig. 3. For θ-AlF_3 the observed shoulder allows an assignment of at least two different lines (see Fig. 3 and Table 2).

Rotor synchronized spin-echo experiments of this sample did not allow a discrimination between different ^{19}F-sites.

For completeness, the ^{19}F and ^{27}Al MAS NMR spectra (central lines) of the compounds used as precursors for the synthesis of κ- and θ-AlF_3 (see Scheme 1) are shown in Fig. S2. Together with Figs. 3 and 4 they demonstrate changes of spectral patterns in going from precursors to AlF_3 phases. The ^{19}F and ^{27}Al MAS NMR spectra of all other precursors used in this work (ACF, $[AlF_2Py_4]^+Cl^-$, β-$AlF_3{\cdot}3H_2O$) were published previously [12,26,27].

In contrast to ^{19}F MAS NMR, noticeable differences become visible applying ^{27}Al MAS NMR (see Fig. 4). Taking two different spinning frequencies, 25 kHz (Fig. 4) and 12 kHz (Fig. S3), local structural variations between different phases are obvious. The positions of the almost symmetrical central lines (see also Table 2) clearly indicate the existence of a sixfold fluorine coordination of Al. The number of different Al-sites and their quadrupolar parameters however, cannot be deduced from central lines. Only for θ-AlF_3 a broadening due to second-order quadrupolar effects

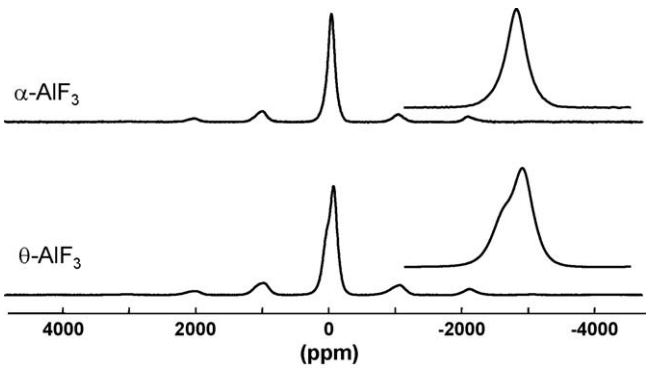

Fig. 3. ^{19}F MAS NMR spectra (ν_{rot} = 25 kHz) of α- and θ-AlF_3 phases; central lines are given with enlarged insert.

Table 2
^{19}F and ^{27}Al MAS NMR parameters of all known crystalline AlF_3 phases as determined by simulation.

Phase	$\delta_{i(19F)}$ [ppm] (FWHM [kHz])	δ_{27Al} [ppm]	ν_Q [kHz] (σ)	η_Q (d)	Comment	Rel. intens. ratio	Ref.
α-AlF_3	−172.6 (3.38)	−16.1	32.0	0.0	cryst.	1	[21]
			34.5	0.0			[20]
			31.8	0.0			[22]
η-AlF_3 (from $[AlF_2Py_4]^+Cl^-$)	−173.0 (3.43)	−13.7	230	0.0	cryst.	1	This work
η-AlF_3 (from ACF)	−173.0 (3.32)	−13.7	230	0.0	cryst.	1	
		−15.4	140 (σ)	3 (d)	distr.	4.5	This work
		−15.4	95 (σ)	3 (d)	distr.	4.5	
β-AlF_3	−172.8 (4.15)	−15.0	120.0	0.8	cryst.	1	[20]
		−15.4	140 (σ)	3 (d)	distr.	1	This work
		−15.4	95 (σ)	3 (d)	distr.	1	
κ-AlF_3	−173.4 (4.20)	−18.9	200 (σ)	3 (d)	distr.	1	This work
		−18.9	160 (σ)	3 (d)	distr.	1	
θ-AlF_3	−171.6 (5.34)	−14.2	390	0.0	cryst.	1.2	This work
		−18.0*	720	0.4	cryst.	1	
		−18.0	700	0.8	cryst.	1	
	−175.3 (2.26)	−15.4	200 (σ)	3 (d)	distr.	4	

Cryst: Al-site with one defined parameter set; distr.: Al-site with distributions of quadrupolar parameters; *position of the signal maximum at −18.7 ppm. σ, d: adjustable parameters of Czjzek-distribution; $d = 3$ as usual for octahedral coordination; σ is given in [kHz] s. also [29].

can be observed. In such cases, reliable information about the quadrupolar parameters can be obtained from the NMR of satellite transitions.

For these purposes satellite transition (SATRAS) NMR spectra were recorded [29]. The extent and the shape of the envelope of the NMR spectrum are approximately determined by the quadrupolar frequency ν_Q and the asymmetry parameter η_Q, respectively. All ^{27}Al SATRAS NMR spectra were calculated for both spinning speeds using the program developed in Le Mans [29]. Results of these calculations are shown exemplarily for κ- and η-AlF_3 in Fig. 5. All ^{27}Al NMR parameters as determined by simulation are summarized in Table 2. Only for α- and η-AlF_3 (prepared from AlF_2Py_4Cl) the simulation of the ^{27}Al SATRAS NMR spectrum was possible with one crystalline Al-site with defined quadrupolar parameters (see Table 2).

All other spectra could only be reproduced taking into account a superposition of Al-sites with fixed and distributed NMR parameters. The number of different Al-sites necessary for the calculation of the ^{27}Al SATRAS spectra of each phase is in agreement with the number of crystallographically sites derived from XRD findings (see Tables 1 and 2). Also β-AlF_3 was

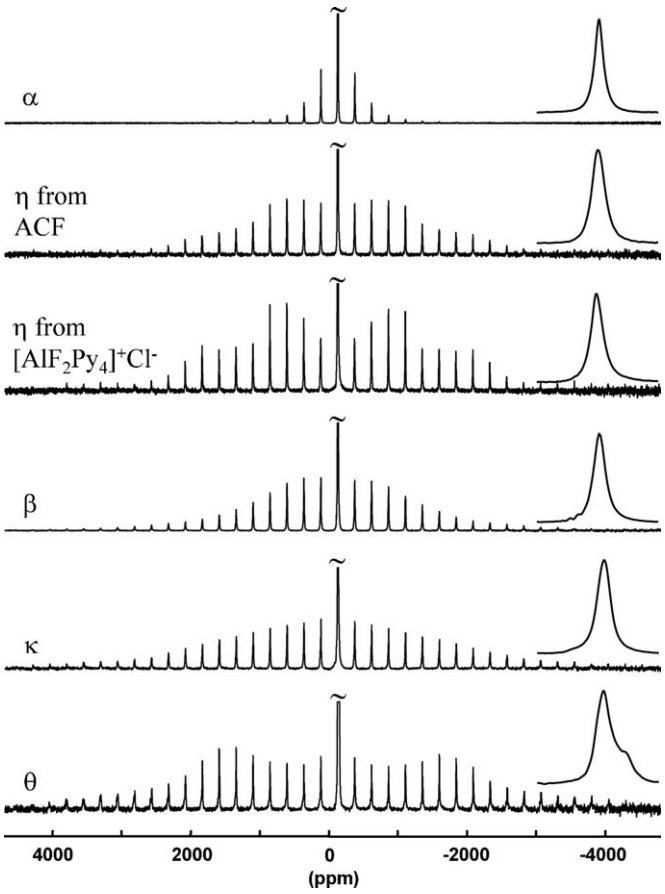

Fig. 4. Experimental ^{27}Al SATRAS NMR spectra of all AlF_3 phases (ν_{rot} = 25 kHz) with the respective central lines given as insets. The labelling of the phases is given directly in the figure.

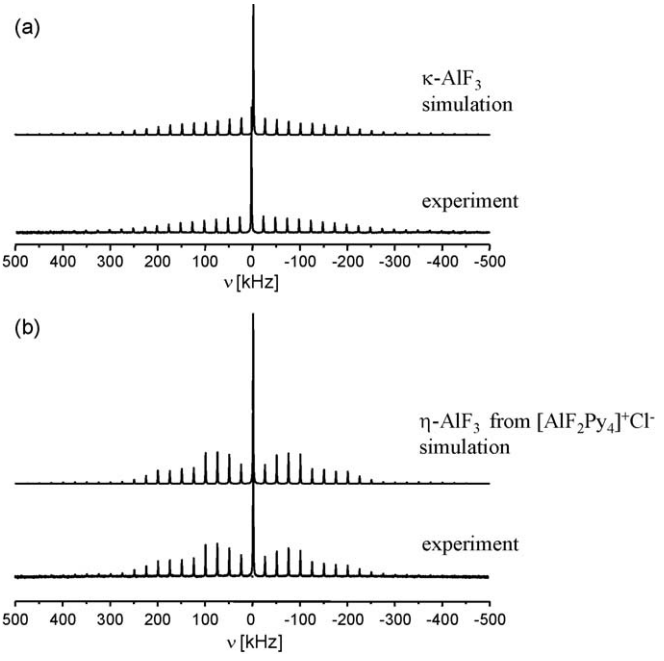

Fig. 5. Experimental (ν_{rot} = 25 kHz) and calculated SATRAS NMR spectra of ^{27}Al for (a) crystalline κ-AlF_3 and (b) crystalline η-AlF_3. The parameters of simulation for the two Al-sites of κ-AlF_3 and one Al-site of η-AlF_3 are given in Table 2.

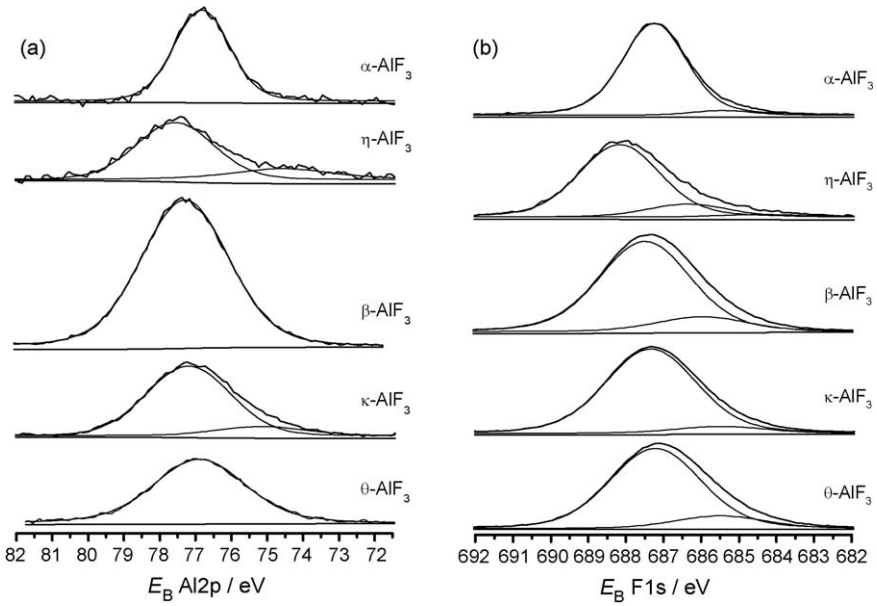

Fig. 6. Al 2p- (a) and F 1s- (b) XP spectra of AlF_3 phases with peak fitting results.

Table 3
Spectroscopic parameters of XPS of crystalline AlF_3 phases: binding (BE) and kinetic energies (KE) of Al and F. Charge reference: C 1s at BE = 284.8 eV. Bold numbers represent the major species.

Phase	Binding energy BE (FWHM) [eV]			Kinetic energy KE [eV]	
	Al 2s	Al 2p	F 1s	Al $KL_{23}L_{23}$	F $KL_{23}L_{23}$
α-AlF_3	121.6 (2.8)	76.7 (1.9)	**687.2 (2.3)** 685.4 (2.3)	1383.2	652.2
η-AlF_3 from ACF	122.2 (3.5) 118.9 (3.5)	77.4 (2.7) 74.4 (4.0)	**688.2 (2.8)** 686.4 (2.8) 684.4 (2.8)	1382.2	651.4
β-AlF_3	122.0 (3.8)	77.1 (3.1)	**687.5 (3.1)** 686.0 (3.1)	1382.5	651.9
κ-AlF_3	121.9 (3.7) 120.2 (3.7)	77.1 (2.7) 75.0 (2.8)	**687.3 (3.1)** 685.5 (3.1)	1382.6	652.2
θ-AlF_3	121.6 (3.5)	76.7 (3.4)	**687.2 (3.1)** 685.5 (3.1)	1383.1	652.4

recalculated now with two crystallographic Al-sites in agreement with XRD unlike to previous work [20].

η-AlF_3, prepared from ACF, cannot be obtained phase pure. Here, small reflections of β-AlF_3 are already visible in the XRD powder pattern (see Fig. 1). Accordingly, the calculation of the ^{27}Al SATRAS NMR spectrum was successful with one crystallographic site superimposed by the two Al-sites of β-AlF_3 with distributed parameters. The reproduction of the experimental ^{27}Al spectrum of θ-AlF_3 requires a superposition of four aluminium sites in an intensity ratio nearly corresponding to the abundance of the different sites in the elemental cell (see Table 2). At least two sites can be discriminated in the ^{27}Al 3QMAS spectrum of θ-AlF_3, the resolution of all four sites is not possible. An ^{19}F–^{27}Al HETCOR MAS NMR experiment revealed one unresolved asymmetric correlation peak, however the Al-sites at $\delta_{27Al} = -18$ ppm seem to correlate more with the F-sites resonating in the highfield part of the ^{19}F MAS NMR spectrum ($\delta_{iso} \approx -175$ ppm) (both not shown here).

Al 2p and F 1s XPS spectra of all AlF_3 phases are shown in Fig. 6a and b. Binding (BE) and kinetic energies (KE) are summarized in Table 3. The binding energies for α- and β-AlF_3 are in good accordance to the binding energies measured by Boese et al. earlier [19]. In the given study F 1s XP spectra are asymmetric to lower BE indicating the coexistence of minor species. The main F 1s component of η-AlF_3 occurs in a significantly higher BE. For the Al 2p XP spectra additional minor low BE species have been found with η- and κ-AlF_3. The FWHM of Al 2p for β-AlF_3 is rather high probably also pointing to coexisting Al species. Another point to be mentioned here is that all XPS data represent the chemistry at the very surface which may contain reaction products of the original phase with ambient atmosphere. All the other methods applied in this study reveal bulk information.

3. Discussion and conclusion

As already indicated in Scheme 1 and in Section 4, the preparation of aluminium fluoride phases, which is possible starting from different precursors, is demanding especially for η-, κ- and θ-AlF_3. The phase purity is not only governed by the quality of the educts but also by a careful compliance of heating and cooling regimes. An extreme example for this situation is the observation of additional reflections in the case of η-AlF_3 after quenching of the sample (see Fig. S1), pretending a new phase. Nevertheless, the preparations performed in this study resulted from an X-ray point of view in aluminium fluoride phases of much

better crystallinity and phase purity as compared to previously published diffractograms [25].

The common feature of all phases, namely corner sharing of AlF_6 octahedra implies only marginal local structural differences and makes their assignment very difficult. The larger structural diversity in the κ- and θ-AlF_3 phases, formed by different arrangements of rings of three, four or five corner-shared AlF_6 octahedra, is reflected both in the number and width of vibrational bands (see Fig. 2) as well as the broad Al 2p and F 1s XPS spectra (Fig. 6). Especially for the XPS spectra, although in the typical range of binding energies for aluminium fluorides, it is hard to extract phase specific information. Even ^{19}F MAS NMR spectra (see Fig. 3) do not allow a discrimination between the different phases as a consequence of the strong homonuclear dipolar coupling which finally covers the resolution of different fluorine sites in the case of β- and κ-AlF_3. For θ-AlF_3 two shoulders can be observed covering 7 fluorine sites present in the matrix.

Only ^{27}Al SATRAS NMR measurements along with the simulation of the spectra allow to work out details of local structural peculiarities. The spectra recorded at rotation frequencies of 25 kHz (see Fig. 4) and 12 kHz (see Fig. S3), respectively, allow both the identification of subtleties for each phase. Furthermore, the spectra are unambiguously different for each phase. In agreement with predictions from XRD (see Table 1) the same number of according Al-sites was necessary for calculation of the ^{27}Al SATRAS spectra.

Except for α- and η-AlF_3, whose spectra were reproduced with one crystallographic Al-site, a superposition of two or more sites was necessary. For some of them distributions of quadrupolar parameters have to be taken into account. The latter can be explained by (ii) the option that parts of the aluminium fluorides are still in the amorphous state, i.e. not visible in the XRD powder patterns, and (i) by channel structures existent in β-, κ- and θ-AlF_3 allowing the adsorption of molecules (e.g. water) which finally influence the electric field gradients acting locally on the aluminium sites. The largest quadrupolar frequencies were obtained for θ-AlF_3 already indicated by the shape of the ^{27}Al central line. The latter is broadened due to second-order quadrupolar effects.

A simulation of the ^{27}Al spectrum of the η-AlF_3 phase prepared from ACF requires a superposition of three signals: one with the parameters from crystalline η-AlF_3 and the two sites from β-AlF_3. Looking at the relative intensity ratio the actual η-AlF_3 phase is discriminated. β-AlF_3 contributions were already visible in the XRD powder pattern (Fig. 1) but it is not clear from XRD how large the additional portion of ^{27}Al in an amorphous environment is.

Summarizing the findings of this study it is obvious that among the spectroscopic techniques used here only the utilization of ^{27}Al SATRAS NMR allowed a clear discrimination between different AlF_3 phases. The quadrupolar parameters of all aluminium sites were determined for the first time for all phases including their distributions if necessary.

In addition, η-AlF_3 was isolated and characterized following a new preparation path different from those known so far in the literature.

4. Experimental

4.1. Sample preparation

α-AlF_3 (white powder) was prepared by thermal decomposition of β-$AlF_3{\cdot}3H_2O$ in a special platinum Q-crucible under self-generated atmosphere at 1000 °C for 2 h [30]. Alternatively, a sample purchased from Aldrich can be used.

β-AlF_3 (white powder) was prepared by thermal decomposition of α-$AlF_3{\cdot}3H_2O$ under self-generating atmosphere by heating to 450 °C (heating rate: 10 °C/min) and holding this temperature for 2 h.

All other aluminium fluoride phases, i.e. η-AlF_3, η-py-AlF_3, κ- and θ-AlF_3 were prepared by heating the respective precursor compound under Schlenk conditions for 30 min at 455 °C (heating rate: 10 K/min). The Schlenk container was positioned horizontally in a tube furnace applying a dynamic vacuum ($p < 10^{-2}$ mbar). As result grey or dark grey powders were obtained.

ACF and $[AlF_2Py_4]^+Cl^-$, respectively, were used as precursor compounds for η-AlF_3 and η-py-AlF_3. The synthesis of both precursor compounds was performed according to the procedure described in the literature. ACF was prepared by adding an excess amount of CCl_3F to solid $AlCl_3$ [12,13]. This reaction is strongly exothermic and needs for control an immersion of solid $AlCl_3$ in inert solvents as e.g. perfluoralkanes. $[AlF_2Py_4]^+Cl^-$ was prepared by dissolution of $AlCl_3{\cdot}3Py$ in pyridine followed by subsequent adding of 3 equiv of Me_3SiF at −20 °C within 2 h as described in [27].

For κ- and θ-AlF_3 the direct precursor compounds were obtained from pyridinium tetrafluoroaluminate ($PyHAlF_4$) (see also Scheme 1). β-NH_4AlF_4 was prepared according to [24]. As included in Scheme 1, both $N(CH_3)_4AlF_4$ and $N(C_2H_5)_4AlF_4$ were taken as precursor compounds for θ-AlF_3. $N(CH_3)_4AlF_4$ was prepared as described by [24] by metathesis from $PyHAlF_4$. $N(C_2H_5)_4AlF_4$ was prepared formerly in our research group.

For $PyHAlF_4$ (pyridine-$HAlF_4$) the synthesis given by [23] was slightly varied:

80 ml/20 ml toluol/pyridine were added to 8 ml (16 mmol) of a 2 M $Al(Me)_3$—solution (Aldrich, solvent: toluol) in a Schlenk container and cooled down to −78 °C using a freezing mixture (dry ice/^{i}PrOH). After that 1.6 ml of a (HF{Pyridine}-solution (Aldrich, 70% HF; 30% Pyridine)) were added in a molar ratio Al:F as 1:4. A vigorous exothermic reaction can be observed immediately. A white precipitate is formed which is densifying with time. After separation from the solvent and drying in vacuum at 70 °C, 3.24 g of a white product, sensitive to hydrolysis, could be isolated, which was identified as $PyHAlF_4$.

4.2. Elemental analysis and XRD

The elemental analysis of the samples was performed with an Euro EA Elemental Analyzer (C, H, N). The fluoride contents were checked with a fluoride sensitive electrode after conversion of the solids with Na_2CO_3/K_2CO_3 into a soluble form. For all fluorides synthesized from organic precursors traces of carbon and hydrogen were determined, the absolute mass percentages did not exceed 0.5% for C and 0.2% for H. The N and Cl mass percentages for the η-AlF_3 phases were determined as 0% N and 0.5% Cl (η-AlF_3 from ACF) and 0% N and 1% Cl for (η-AlF_3 from $[AlF_2Py_4]^+Cl^-$). However, the F-contents of the AlF_3-samples determined with our "routine"-method varied from 60% to 66% (ideal 68%) which is possibly due to an incomplete conversion, masking or differences in the well known water adsorption on aluminium fluorides.

The presented X-ray diffractograms were measured on a Seifert XRD3003TT diffractometer with Cu Kα radiation.

4.3. Solid state NMR

^{19}F and ^{27}Al NMR spectra were recorded on a Bruker AVANCE 400 spectrometer (Larmor frequencies: ν_{19F} = 376.4 MHz; ν_{27Al} = 104.3 MHz) using a 2.5 mm MAS probe (Bruker Biospin).

^{19}F MAS NMR ($I = 1/2$) spectra were recorded with a $\pi/2$ pulse duration of $p1$ = 2.0 μs, a spectrum width of 400 kHz, and a recycle delay of 3 s for all samples. Spectral changes for longer recycle delays were checked. The isotropic chemical shifts δ_{CS} of ^{19}F resonances are given in respect to the $CFCl_3$ standard. Existing

background signals of ^{19}F could be completely suppressed with the application of a phase-cycled depth pulse sequence according to Cory and Ritchey [31].

^{27}Al MAS NMR ($I = 5/2$) spectra were recorded with an excitation pulse duration of 1 μs. The chemical shifts of ^{27}Al are given with respect to $AlCl_3$ in aqueous solution (0 ppm). The recycle delay was chosen as 1 s. Two different rotation frequencies, 25 and 12 kHz, were used. For the ^{27}Al SATRAS NMR spectra the magic angle was accurately set by minimization of the line width of the side bands of ^{51}V in NH_4VO_3 powder. Symmetric ^{27}Al SATRAS spectra were obtained after correction with the function determined for the probe in dependence on the excitation frequency. The simulation of the ^{27}Al SATRAS NMR spectra was performed with the program developed by Buzaré and co-workers [29] in Le Mans (France).

4.4. IR

Fourier transform infrared spectra (FT IR) were recorded using KBr disks (4000–400 cm^{-1}) or CsI disks (700–200 cm^{-1}) on a Perkin-Elmer 2000 spectrometer in transmission mode. About 1–2 mg of sample was ground with about 400 mg of KBr (about 200 mg of CsI) and pressed ($p = 5$ t). Spectra were measured in wave number ranges of 200–700 cm^{-1} and 400–4000 cm^{-1} at room temperature.

4.5. XPS

All XPS and XAES data were measured with a VG Escalab 200× at the Federal Institute for Materials Research and Testing (BAM, Berlin, Germany). Non-monochromatic Mg Kα X-ray radiation (1253.6 eV) was used for excitation. Electrons were detected by a hemispherical analyzer using a fixed retard ration (FRR-mode) of 10 for survey scans and fixed analyzer transmission (FAT-mode) of 20 eV for high resolution spectroscopy. The spectrometer energy scale was calibrated using the procedure and binding energy reference data recommended by ISO (ISO 15472:2001). Charge referencing was carried out using the C 1s binding energy (284.8 eV).

The investigated powders were fixed on a standard specimen holder by double adhesive tape.

For background correction a Shirley background [32] was applied to all spectra. High resolved spectra were examined by peak fitting using a peak shape model with convolution of Gaussians and Lorentzians and the *Unifit 2004* software [33].

Acknowledgements

Sincere thanks go to Prof. J.Y. Buzaré (Le Mans, France) for the possibility to use the SATRAS program developed in his group at the Université du Maine.

M. Balski and I. Hartwich are kindly acknowledged for the preparation of η-AlF_3 and its precursor samples, respectively, and S. Bäßler and Dr. A. Zehl for the elemental analysis.

We thank Prof. J. Kneipp and Dr. P. Emmerling (BAM Berlin) for several Raman tests and fruitful discussions.

Appendix A. Supplementary data

Supplementary data associated with this article can be found, in the online version, at doi:10.1016/j.jfluchem.2009.10.015.

References

[1] J. Ravez, A. Mogus-Milankovic, J.P. Chaminade, P. Hagenmuller, Mater. Res. Bull. 19 (1984) 1311–1316.
[2] P. Daniel, A. Bulou, M. Rousseau, J. Nouet, J.L. Fourquet, M. Leblanc, R. Burriel, J. Phys. Condens. Matter 2 (1990) 5663–5677.
[3] P. Daniel, A. Bulou, M. Rousseau, J. Nouet, Phys. Rev. B42 (1990) 10545–10552.
[4] P. Daniel, Thesis, Université du Maine, Le Mans, France, 1990.
[5] G. Scholz, R. Stösser, J.Y. Buzaré, C. Legein, G. Silly, Appl. Magn. Res. 18 (2000) 199–215.
[6] P.J. Chupas, S. Chaudhuri, J.C. Hanson, X. Qiu, P.L. Lee, S.D. Shastri, S.J.L. Billinge, C.P. Grey, J. Am. Chem. Soc. 126 (2004) 4756–4757.
[7] A. Hess, E. Kemnitz, J. Catal. 149 (1994) 449–457.
[8] A. Hess, E. Kemnitz, A. Lippitz, W.E.S. Unger, D.H. Menz, J. Catal. 148 (1994) 270–280.
[9] E. Kemnitz, D.-H. Menz, Progr. Solid State Chem. 26 (1998) 97–153.
[10] E. Kemnitz, J. Winfield, in: T. Nakajima, B. Zemva, A. Tressaud (Eds.), Adv. Inorg. Fluorides, Elsevier, 2000, pp. 367–401.
[11] U. Groß, S. Rüdiger, E. Kemnitz, K.-W. Brzezinka, S. Mukhopadhyay, C. Bailey, A. Wander, N. Harrison, J. Phys. Chem. A 111 (2007) 5813–5819.
[12] T. Krahl, R. Stösser, E. Kemnitz, G. Scholz, M. Feist, G. Silly, J.-Y. Buzaré, Inorg. Chem. 42 (2003) 6474–6483.
[13] T. Krahl, E. Kemnitz, J. Fluorine Chem. 127 (2006) 663–678.
[14] B. Boulard, C. Jacoboni, M. Rousseau, J. Solid State Chem. 80 (1989) 17–31.
[15] S.L. Schroeder, N. Weiher, Phys. Chem. Chem. Phys. 8 (2006) 1807–1811.
[16] I. Grohmann, A. Hess, E. Kemnitz, W. Fentrup, W.E.S. Unger, J. Wong, M. Rowen, T. Tanaka, M. Froba, J. Mater. Chem. 8 (1998) 1453–1457.
[17] C.D. Wagner, A.V. Naumkin, A. Kraut-Vass, J.W. Allison, C.J. Powell, J.R. Rumble Jr., NIST Standard Reference Database 20, Version 3. 5, 2007.
[18] O. Boese, W.E.S. Unger, E. Kemnitz, S.L.M. Schroeder, Phys. Chem. Chem. Phys. 4 (2002) 2824–2832.
[19] O. Boese, E. Kemnitz, A. Lippitz, W.E.S. Unger, Fresen. J. Anal. Chem. 358 (1997) 175–179.
[20] P.J. Chupas, M.F. Ciraolo, J.C. Hanson, C.P. Grey, J. Am. Chem. Soc. 123 (2001) 1694–1702.
[21] G. Silly, C. Legein, J.Y. Buzaré, F. Calvayrac, Solid State NMR 25 (2004) 241–251.
[22] G. Scholz, O. Korup, Solid State Sci. 8 (2006) 678–684.
[23] N. Herron, D.L. Thorn, R.L. Harlow, F. Davidson, J. Am. Chem. Soc. 32 (1993) 3028–3029.
[24] N. Herron, D.L. Thorn, R.L. Harlow, G.A. Jones, J.B. Parise, J.A. Fernandez-Baca, T. Vogt, Chem. Mater. 7 (1995) 75–83.
[25] N. Herron, W.E. Farneth, Adv. Mater. 8 (1996) 959–968.
[26] E. Kemnitz, U. Groß, S. Rüdiger, G. Scholz, D. Heidemann, S.I. Troyanov, I.V. Morosov, M.H. Lemée-Cailleau, Solid State Sci. 8 (2006) 1443–1452.
[27] A. Dimitrov, D. Heidemann, E. Kemnitz, Inorg. Chem. 45 (2006) 10807–10814.
[28] A. Le Bail, J.L. Fourquet, U. Bentrup, J. Solid State Chem. 100 (1992) 151–159.
[29] G. Scholz, R. Stösser, J. Klein, G. Silly, J.Y. Buzaré, Y. Laligant, B. Ziemer, J. Phys.: Condens. Matter 14 (2002) 2101–2117.
[30] D.H. Menz, U. Bentrup, Z. Anorg. Allg. Chem. 576 (1989) 186–196.
[31] D.G. Cory, W.M. Ritchey, J. Magn. Reson. 80 (1988) 128–132.
[32] D.A. Shirley, Phys. Rev. B 5 (1972) 4709–4714.
[33] R. Hesse, P. Streubel, R. Szargan, Surf. Interface Anal. 37 (2005) 589–607.
[34] A. LeBail, F. Calvayrac, J. Solid State Chem. 179 (2006) 3159–3166.
[35] JCPDS-ICCD-International Centre for Diffraction Data: PDF-2 Database, USA, Release 2001.